Journal of Applied Physics

RESEARCH ARTICLE | JUNE 27 2024

Ab initio melting curve of body-centered cubic bismuth

Leonid Burakovsky ; Daniel A. Rehn ; Simone Anzellini ; Daniel Errandonea

J. Appl. Phys. 135, 245104 (2024)
https://doi.org/10.1063/5.0213734

Journal of Applied Physics ARTICLE pubs.aip.org/aip/jap

Ab initio melting curve of body-centered cubic bismuth

Cite as: J. Appl. Phys. **135**, 245104 (2024); doi: 10.1063/5.0213734
Submitted: 12 April 2024 · Accepted: 10 June 2024 ·
Published Online: 27 June 2024

Leonid Burakovsky,[1,a)] Daniel A. Rehn,[1] Simone Anzellini,[2] and Daniel Errandonea[2]

AFFILIATIONS

[1]Los Alamos National Laboratory, Los Alamos, New Mexico 87545, USA
[2]Departamento de Física Aplicada-ICMUV, MALTA Consolider Team, Universidad de Valencia, Edificio de Investigación, C/Dr. Moliner 50, Burjassot, 46100 Valencia, Spain

[a)]**Author to whom correspondence should be addressed:** burakov@lanl.gov

ABSTRACT

Body-centered cubic bismuth (bcc-Bi) has long been considered an ideal pressure standard/calibrant; thus, the accurate knowledge of both its equation of state (EOS) and melting curve is of primary importance for future high pressure and high temperature experiments. However, its melting curve has never been measured experimentally beyond 5 GPa, and several theoretical calculations do not agree with each other and, in fact, differ by as much as a factor of 2 with regard to the bcc-Bi melting point at 50 GPa. Here, we present the calculation of the melting curve of bcc-Bi to 400 GPa via quantum molecular dynamics simulations using the Z method implemented with VASP. We also present the *ab initio* EOS of bcc-Bi as well as its principal Hugoniot, which both appear to be in excellent agreement with the available experimental data. At 100 GPa, the temperature extent (from zero to melt) of bcc-Bi is comparable to that of gold. At pressures of $>\sim$500 GPa, the melting curve of bcc-Bi is (quasi-)parallel to, being $\sim$1000 K below that of rhenium, the highest melter above $\sim$30 GPa among the elements of the third row of the periodic table, which makes bcc-Bi the second highest melter behind Re.

INTRODUCTION

Bismuth (Bi) is one of the most interesting elements that exist in nature. Because of its peculiar three-dimensional Dirac dispersion, Bi possesses a number of unique physical properties such as diamagnetism and high magnetoresistance. Several important phenomena such as the Seebeck, Ettingshausen–Nernst, Shubnikov–de Haas, and de Haas–van Alphen effects were first observed in Bi.[1] At ambient conditions, the crystal structure of Bi is rhombohedral and results from a minor deformation of a cubic lattice. This gives rise to Bi being a semimetal as well as its band structure being explained by the deformation model.[2] However, Bi nanoclusters are semiconductors and can be used as building blocks for the construction of novel materials.[2]

Bi is of high interest to phase-diagram studies. Its own phase diagram is relatively complex at low pressure (P) and consists of five different solid structures shown in Fig. 1. At ambient temperature (T), with increasing P, a sequence of solid–solid structural phase transitions occurs: A7 rhombohedral ($R\bar{3}m$) Bi-I–C-centered monoclinic ($C2/m$) Bi-II–body-centered tetragonal (bct) incommensurate host–guest Bi-III–body-centered cubic (bcc) Bi-V for which all the transition points are well known and have been widely used as pressure calibration points. The P–T phase diagram of Bi has multiple triple points shown in Fig. 1 such as the IV–V-liquid one at (P, T) = (3.8 GPa, 569 K).[4] Bi-IV, another solid phase on its phase diagram, has orthorhombic ($oC16$) *Cmca* structure. The bcc Bi-V is stable in an exceptionally wide pressure (P) interval from 7.6 $\pm$ 0.6 (Table 1 of Ref. 5) up to at least 300 GPa.[6] Hence, above $\sim$10 GPa, the phase diagram of Bi is relatively simple: just one solid (bcc) and liquid phases. In addition, Bi is a high-Z element yet nonradioactive (in fact, it has the highest Z among all the nonradioactive elements), thus it provides a strong x-ray diffraction (XRD) signal, which is straightforward to measure. The bulk modulus of bcc-Bi ($\sim$55 GPa) is much smaller than that of most of the pressure standards, e.g., Au (167 GPa), Pt (277 GPa), Ta (194 GPa), W (296 GPa);[7] therefore, under the same P, its

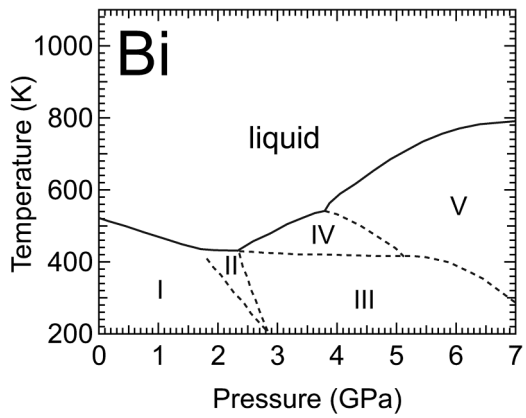

FIG. 1. The low-P portion of the phase diagram of Bi. The figure reproduces Fig. 1(a) of Ref. 3.

volume change will be larger and, thus, the precision of the determination of P is higher. Also, its yield strength is much smaller than that of other pressure standards, and, therefore, in static compression experiments, its uniaxial stress components, t, are much smaller, e.g., comparison of the values of t of Bi to those of both Cu and Au[6] shows an order of magnitude difference. Thus, bcc-Bi appears to be more hydrostatic than most of the other pressure standards. All this makes bcc-Bi essentially an ideal pressure standard and pressure calibrant. Note that Bi has been used as a P calibrant even at low pressures, e.g., in the study on the low-P phase diagram of Sn.[8]

However, the phase diagram of Bi above 10 GPa, specifically, its melting curve, is essentially unknown. The melting curve of Bi has never been measured beyond ∼5 GPa.[9] Experimental data at higher P are limited to shock compression along the principal Hugoniot and release, which can only constrain the melting curve in a narrow P range. In Ref. 10, the melting on the Hugoniot of Bi is estimated to occur between ∼30 GPa and 2300 K and 45 GPa and 2600 K. In Ref. 11, however, these values are ∼18 GPa and 1250 K and 28 GPa and 1700 K. This latter set of values is in agreement with the theoretical calculation of Ref. 12. There are several theoretical studies on the melting curve of Bi to as high as 80 GPa,[12] but the results of these studies do not agree with each other. Specifically, at a pressure of 50 GPa, the following melting temperatures (T_m) are predicted (in K): 1645,[13] ∼1950,[14] ∼2700,[15,16] ∼2750,[12] and ∼3300,[17] so that the lowest and highest of these T_ms differ from each other by a factor of 2. [We note that in our simulations, we discuss in detail what follows T_m (50 GPa) ∼3200 K.] Hence, the melting curve of bcc-Bi remains virtually unknown. The purpose of our present study is the very accurate calculation of this melting curve using first-principles based quantum molecular dynamics (QMD) simulations. To have a reliable pressure standard/calibrant, the knowledge of both its equation of state (EOS) and melting curve is indispensable. The accurate EOS of bcc-Bi known from the experiment will be complemented by our theoretical results on its melting curve for the complete (ideal) bcc-Bi pressure standard.

METHODS

Our theoretical study of the melting curve of bcc-Bi was carried out using VASP (Vienna *Ab initio* Simulation Package).[18,19] The electron core–valence structure of Bi was chosen to be [^{54}Xe $4f^{14}$] $5d^{10}$ $6s^2$ $6p^3$, i.e., the 15 outermost electrons of Bi were assigned to the valence. The valence electrons were represented by a plane wave basis set with a cutoff energy (ENCUT in VASP) of 450 eV (following Ref. 20), while the core electrons were represented by projector augmented-wave (PAW) pseudopotentials. The generalized gradient approximation (GGA) with the Perdew–Burke–Ernzerhof (PBE) exchange-correlation functional[21] was chosen for our theoretical study.

A comprehensive analysis of the application of DFT-based methods to Bi was carried out in Ref. 22, including comparison of the outcome produced by LDA (local density approximation), GGA-PBE, GGA-PBEsol (the revised PBE, Ref. 23), RPBE, PW91, AM05, as well as the effect of the inclusion of spin–orbit coupling (SOC); in VASP, it is turned on by LSORBIT, which required the use of the vasp_ncl executable instead of vasp_std or vasp_gam for a single Γ-point. Other meta-GGA DFT functionals such as TPSS, M06-L, MS, SCAN, etc., were also examined.[24] It was concluded that, compared to the experimental lattice constants, EOS parameters, and relative energies of the five solid phases of Bi shown in Fig. 1, GGA-PBE performs the best of all the DFT methods. This was independently confirmed in several theoretical studies; see, e.g., Refs. 20 and 25–27. As regards spin–orbit coupling, it was concluded that, although it is a must to adequately describe the complex phase diagram of Bi as low P and its physical properties,[26–29] especially those of Bi-I, e.g., large spin conversion anisotropy and the anisotropic g-factor[30] as well as anisotropic thermal expansion and zero-T elastic constants.[31] However, with increasing P, the effect of SOC quickly diminishes and virtually disappears for Bi-V (bcc-Bi), which was confirmed in numerous theoretical studies; see, e.g., Refs. 14, 32, and 33. We checked the effect of adding SOC on our theoretical $T = 0$ EOS of Bi: at a given volume, the resulting P is altered by less than 1% at all volumes considered. Hence, SOC can be very safely neglected.

The core radius (the largest value of RCUTs among those for each of the quantum orbitals) of this 16-electron pseudopotential is 2.5 a.u. or 1.323 Å. Since numerical errors in the calculations using VASP remain almost negligible until the nearest neighbor distance reaches $2 \times \mathrm{RCUT}/(1.25 \pm 0.05)$,[34] with this pseudopotential, one can study systems with densities up to ∼60 g/cm^3 (a pressure of ∼5 TPa).

Equations of state

Cold ($T = 0$) EOS of bcc-Bi, in the form of pressure as a function of density, $P = P(\rho)$, was calculated for a bcc unit cell with lattice parameter varying from 4.0 to 2.75 Å with an increment of 0.05 Å, i.e., for a total of 26 points. The corresponding P interval is ∼0–800 GPa. A very dense k-point mesh of $75 \times 75 \times 75$ was used in each case.

Melting simulations

Our quantum molecular dynamics (QMD) melting simulations of bcc-Bi were carried out using the (direct) Z method

implemented with VASP, which is described in detail in Refs. 35–37. QMD simulations are done in the $N\,V\,E$ (number of atoms–volume–energy) ensemble such that (i) V = const., ensures that the final states of these simulations form the corresponding Z isochore and (ii) with E = const., melting is associated with a drop in T and an increase in P, which occur simultaneously (more detail is given below). A total of 10 melting points are obtained, for the lattice constants of bcc-Bi of 3.0–3.95 Å (pressures of ∼0–400 GPa). We used a 432-atom ($6 \times 6 \times 6$) supercell for all the lattice constants except 3.95 Å for which we used a 686-atom ($7 \times 7 \times 7$) supercell, with a single Γ-point in each case; with such large supercells, full energy convergence, to <∼1 meV/atom, was achieved in every case considered. A time step of 1 fs was used for all the lattice constants except 3.95 Å for which a time step of 1.5 fs was used. The reasons for choosing a much large supercell and a large time step in the 3.95 Å case are discussed below. We performed an average of five computer runs per point, for a total of ∼50 computer runs. For each of these runs, the total simulation length was 17500–25000 time steps (15000–17500 in the 3.95 Å case), so that the maximum total simulation running time was ∼25 ps in either case.

RESULTS

Cold equation of state of bcc-Bi

Fitting the results on $P = P(V)$ of our cold EOS calculations with the third-order Birch–Murnaghan (BM3) EOS[38,39] of the form [in the following B and B' are bulk modulus, in GPa, and its P-derivative, respectively; ρ is the density, in g cm^{-3}; and the subscript 0 means ($T = 0$, $P = 0$)]

$$P(\rho) = \frac{3}{2} B_0 \left(\eta^{7/3} - \eta^{5/3}\right)\left[1 + \frac{3}{4}(B_0' - 4)\left(\eta^{2/3} - 1\right)\right], \quad (1)$$

where $\eta = \rho/\rho_0$, results in the following set of parameters for bcc-Bi:

$$\rho_0 = 11.1, \quad B_0 = 55.1(2.1), \quad B_0' = 4.5(1).$$

Here, the uncertainties in the values of B_0 and B_0' are assigned based on the criterion that variations in these parameters do not move the resulting fit outside the 2σ interval, σ being the standard deviation.

This BM3 analytic form is expected to be reliable to ∼0.8 TPa. Our values of ρ_0, B_0 and B_0' virtually coincide with (11.07(16), 54.3(2.3), 4.56(7)) from *ab initio* calculations on bcc-Bi of Ref. 14 and are in good agreement with the experimental bcc-Bi values (11.49(2), 54.74(29), 4.905(19)) of Ref. 40 and (10.71, 52, 4.6) of Ref. 41 (in fact, our ρ_0 is right in the middle of the above two values that agree with each other to within 7%). Note that neither of the two most recent papers on the EOS of Bi, Refs. 6 and 42, offers the numerical values of the EOS parameters for bcc-Bi.

In Fig. 2, our theoretical cold EOS for bcc-Bi is compared to the experimental EOSs of Refs. 6, 40, and 42. As clearly seen, agreement between theory and experiment is extremely good.

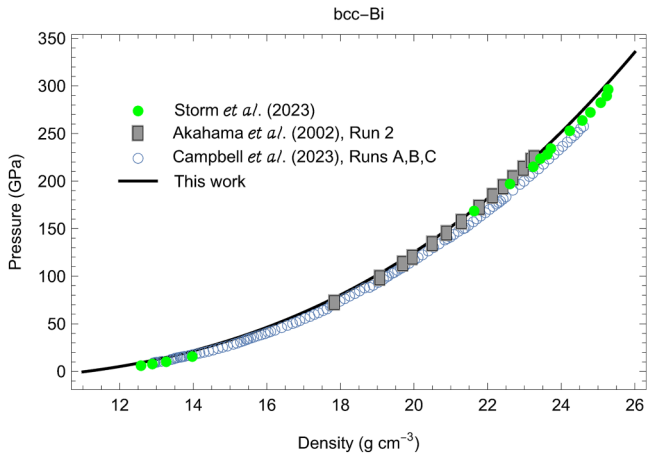

FIG. 2. Comparison of our *ab initio* $T = 0$ EOS of bcc-Bi (this work) to the experimental EOSs of Refs. 6, 40, and 42.

"Thermal" equation of state of bcc-Bi

The finite-T counterpart of the above EOS can be written approximately as

$$P(\rho, T) = P(\rho) + \beta\, T, \quad \beta = 5.6 \times 10^{-3}\ \text{GPa/K}. \quad (2)$$

The value of β in Eq. (2) was chosen to match the initial point on the bcc-Bi melting curve in the ρ–T coordinates (11.221, 569) obtained from the extrapolation of our QMD data $T_m = T_m(\rho)$ are listed in Table I.

This form of the thermal EOS does not take into account explicitly the T-dependence of the bulk modulus, and/or the P- (or T-)dependence of the thermal expansivity, and is, therefore, approximate. Indeed, since

$$P(T, V) = P(T_0, V) + \int_{T_0}^{T} \alpha B_T\, dT,$$

where T_0 is a reference T, α is the volumetric thermal expansion coefficient, and B_T is the isothermal bulk modulus at temperature T, Eq. (2) results from the above relation (with $T_0 = 0$) provided that $\alpha \cdot B_T \approx$ const., i.e., a potential weak T-dependence of B is compensated by a similar weak dependence of α to keep their product (roughly) T-independent. In the case of bcc-Bi, the values of both α and B_T (at low T) are tabulated in Ref. 43 for the three solid phases Bi-III, Bi-IV, and Bi-V and its liquid phase as averages over narrow P intervals. It appears that for bcc Bi-V, the values of $(\alpha \cdot B_T)$ are 6.21×10^{-3}, 6.08×10^{-3}, and 5.90×10^{-3}, so that $(\alpha \cdot B_T) = 6.06 \times 10^{-3}$ to within 2.5%. For the liquid, $(\alpha \cdot B_T) = 4.37 \times 10^{-3}$ to within 3.5%. Since Eq. (2) is meant to extrapolate between $T = 0$ and T_m (at a given ρ), its value of β of 5.6×10^{-3} is reasonable as it is right in between the solid and liquid values; in fact, $\beta \approx 2/3\,(\alpha B_T)_{\text{solid}} + 1/3\,(\alpha B_T)_{\text{liquid}}$. It is

TABLE I. The ten *ab initio* melting points of bcc-Bi, (P_m, $T_m \pm \Delta T_m$), obtained from the Z method implemented with VASP.

lattice constant (Å)	density (g/cm^3)	P_m (GPa)	P_m from Eqs. (1) and (2) (GPa)	T_m (K)	ΔT_m (K)
3.95	11.262	4.37	4.462	650	31.25
3.75	13.161	24.5	24.72	1950	62.5
3.60	14.876	48.1	48.78	3110	87.5
3.50	16.188	72.0	72.10	4110	125.0
3.40	17.658	103	103.1	5230	156.25
3.30	19.313	146	145.6	6630	187.5
3.20	21.181	204	203.7	8340	250.0
3.10	23.297	284	284.0	10 470	375.0
3.05	24.462	335	335.2	11 720	500.0
3.00	25.705	396	395.7	13 130	625.0

interesting to note that the values of $(\alpha \cdot B_T)$ for Bi-III and Bi-IV are, respectively, $\approx 7.5 \times 10^{-3}$ and $\approx 6.0 \times 10^{-3}$.

Albeit being approximate, Eq. (2) is relatively simple and allows one to easily estimate the value of ρ at the corresponding P and T. For instance, comparison of the values of the melting P (P_m) that this "thermal EOS" gives while using the corresponding ρs and T_ms to those that come directly from QMD melting simulations clearly demonstrates that Eq. (2) is virtually exact along the melting curve of bcc-Bi. This comparison can be found in Table I.

Melting curve of bcc-Bi

We found out that the use of a 432-atom bcc-Bi supercell with a lattice constant of 3.95 Å does not ensure accurate QMD results because the corresponding melting simulations exhibit a signature of a mechanical instability, namely, during the QMD runs of bcc-Bi both P and T drift away from their average values determined by the corresponding P-T conditions of the run. This may be the consequence of the facts that (i) bcc-Bi is mechanically unstable when its lattice constant is ~3.95 Å, ($P \sim 4$ GPa) and (ii) unless it is fully mechanically stable, a supercell of a size larger than the critical one is required to simulate its thermodynamic behavior correctly.

According to Ref. 14, bcc-Bi is mechanically unstable below ~8 GPa at low T. That is, the mechanical stability of bcc-Bi occurs simultaneously with its thermodynamic stability at the Bi-III–Bi-V transition (see Fig. 1). Then, most likely, the Bi-III–Bi-V transition line is virtually identical to the bcc-Bi mechanical stability boundary in the T–P coordinates on and above which it is mechanically stable. The treatment of bcc-Fe of Ref. 44 gives a good example of the critical size of the supercell for the correct description of the temperature-stabilized bcc structure: a supercell of at least 1024-atom ($8 \times 8 \times 8$) is required for bcc-Fe. In our case, such a critical size may be $7 \times 7 \times 7$, since the signature of a mechanical instability disappears for a larger 686-atom ($7 \times 7 \times 7$) supercell, which we used for our simulations of bcc-Bi with a lattice constant of 3.95 Å. Since for this supercell the total number of valence electrons exceed 10 000, QMD simulations become extremely time consuming. Hence, a time step of 1.5 fs was chosen in this case in order to partly offset their computational cost.

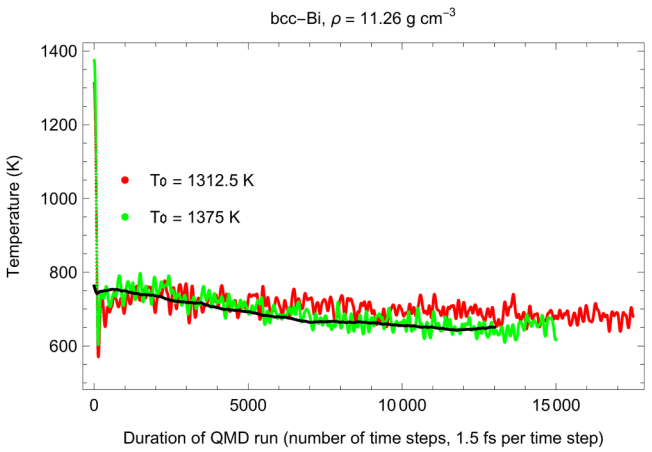

FIG. 3. The melting point (4.4 GPa, 650 K) of bcc-Bi at a density of 11.26 g cm^{-3}: melting T from *ab initio* Z method implemented with VASP. T_0 stands for the initial T of the corresponding QMD run. The black curve is running average T for the $T_0 = 1375$ K run.

The pairs of Figs. 3 and 4 and 5 and 6 offer examples of our Z method melting simulations. They correspond to the first and fifth of the ten T_ms from Table I and demonstrate the time evolution of T and P, respectively, during the corresponding computer runs.

Figures 5 and 6 exemplify the behavior of T and P, respectively, during a QMD run. In what follows, T_0 stands for the initial T of a QMD run. During the entire $T_0 = 1250012\,500$ K run, the system remains a superheated solid since during the 25 ps of running time both the average T and P do not change. Melting

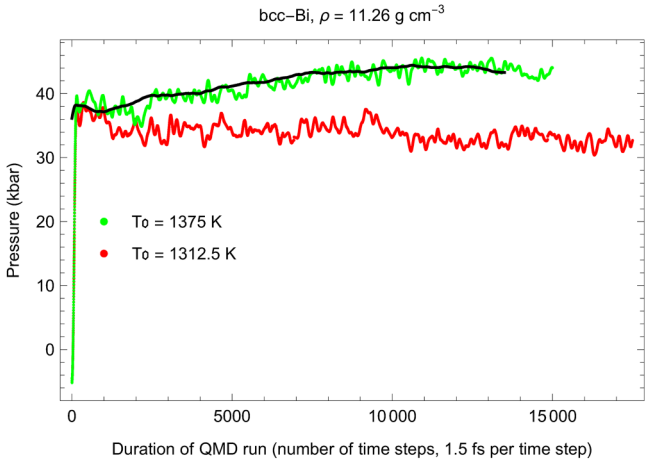

FIG. 4. The same as in Fig. 3 for melting P (in kbar; 10 kbar = 1 GPa). The black curve is running average P for the $T_0 = 1375$ K run.

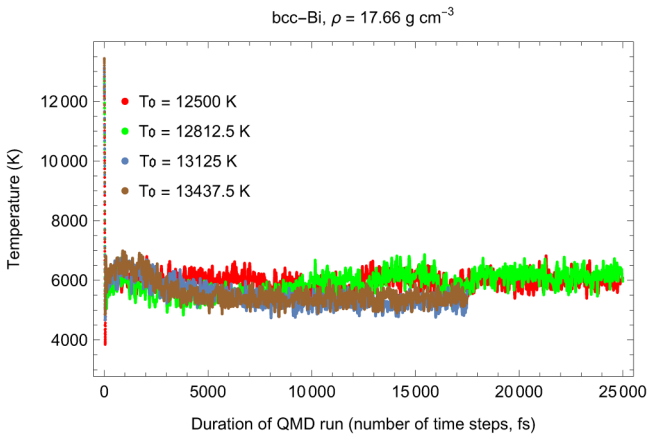

FIG. 5. The melting point (103 GPa, 5230 K) of bcc-Bi at a density of 17.66 g cm^{-3}: melting T from *ab initio* Z method implemented with VASP. T_0 stands for the initial T of the corresponding QMD run.

occurs during the $T_0 = 1312513\,125$ K run: it starts after ∼2.5 ps of running time and shows up as the decrease of average T from ∼6500 to 5230 K and the corresponding increase of average P from ∼101 to 103 GPa; the melting process takes about 3 ps. The simultaneous increase in T and decrease in P happen because during the QMD run the total energy, $E \sim k_B T + P V$, is conserved, and V is fixed. For the same reason, Figs. 5 and 6 appear to be "mirror images" of each other; see Ref. 37 for more detail. In the $T_0 = 1250012\,500$ K run, melting starts after 2 ps of running time, but for higher T_0, it will start even faster, sometimes immediately after the beginning of the QMD run. It is interesting to note that in the $T_0 = 1281212\,812.5$ K run, the system appears to start melting but to revert to solid at a later time and to remain solid for the rest of the run. This phenomenon is rather rare in the QMD melting

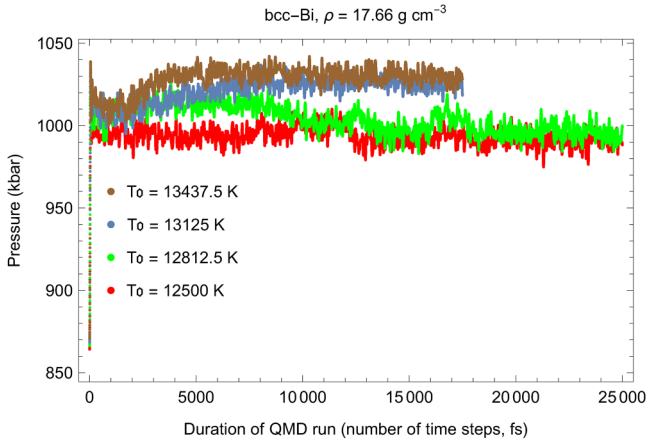

FIG. 6. The same as in Fig. 5 for melting P (in kbar; 10 kbar = 1 GPa).

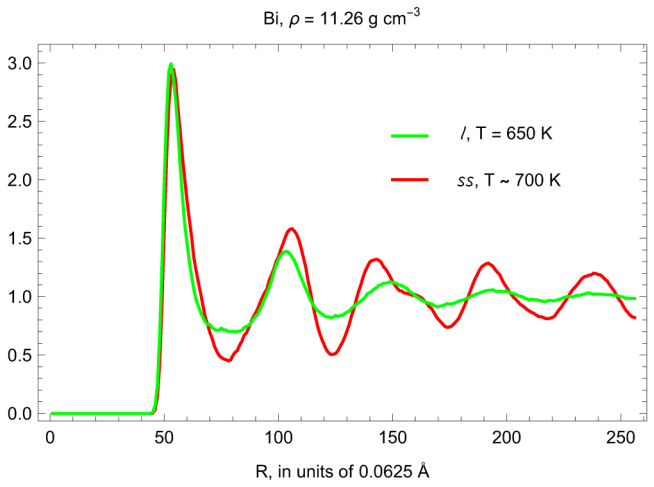

FIG. 7. Radial distribution functions (RDFs) of equilibrium states of bcc-Bi in the QMD Z-method runs of Figs. 2 and 3. The equilibrium temperatures of the superheated (*ss*) and liquid (*l*) final states are indicated as the corresponding Ts.

simulations (it did not occur during the simulations of each of the remaining nine melting points); this is the reason for choosing Figs. 5 and 6 as an example.

In addition to a very clear signature of melting, i.e., the simultaneous decrease of T and increase of P, as in Figs. 3–6, melting was confirmed by (i) examining whether the atomic coordinates form ordered or disordered arrays (in XDATCAR files) and (ii) calculating the corresponding radial distribution functions (RDFs). The RDFs of the final states of the QMD Z-method runs of Figs. 3 and 4 are shown in Fig. 7. It is clearly seen that the $T_0 = 1312.5$ K run results in a superheated solid at $T \sim 700$ K, while the final state of the $T_0 = 1375$ K run is liquid at $T = 650$ K.

The results of our melting simulations are summarized in Table I. The errors in melting T (T_m) are half of the increment of the initial T for a series of computer runs at the corresponding density.[37] We chose these increments to be 62.5, 125, 175, 250, 312.5, 375, 500, 750, 1000, and 1250 K for the first, second,…, and tenth point. The corresponding T_m errors are listed in the table as ΔT_m. The errors in melting P (P_m) are negligibly small of order 1–2 GPa for each point. Included in Table I are also the values of P_m that come from the thermal EOS (1),(2) at the corresponding T_ms.

The best fit of the Simon–Glatzel (SG) form $T_m(P) = T_{m,\mathrm{ref}}\left[1 + \frac{P - P_{\mathrm{ref}}}{a}\right]^b$ to the ten QMD datapoints of Table I represents the corresponding melting curve. Here, $(P_{\mathrm{ref}}, T_{m,\mathrm{ref}})$ is the reference melting point. The best fit of the above SG form ten T_ms of Table I found using Mathematica is

$$T_m^{\mathrm{bcc\text{-}Bi}}(P) = 568.9\left(1 + \frac{P - 3.79}{4.05}\right)^{0.685}. \quad (3)$$

Interestingly enough, the reference point of Eq. (3) at $(P_{\mathrm{ref}}, T_{m,\mathrm{ref}})$

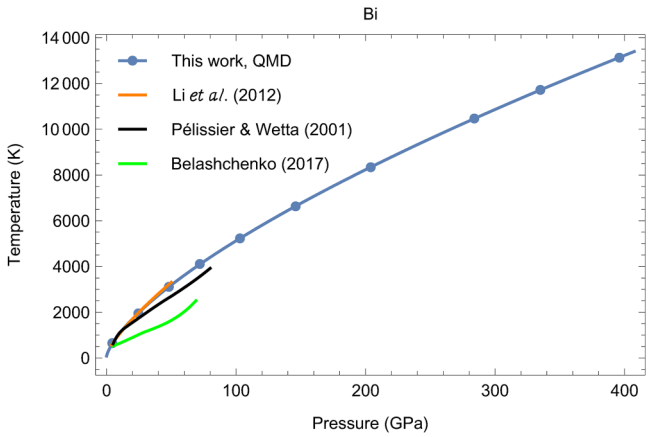

FIG. 8. Comparison of our *ab initio* melting curve of bcc-Bi to the theoretical melting curves available in the literature: Pélissier & Wetta,[12] Belashchenko,[13] and Li *et al.*[17]

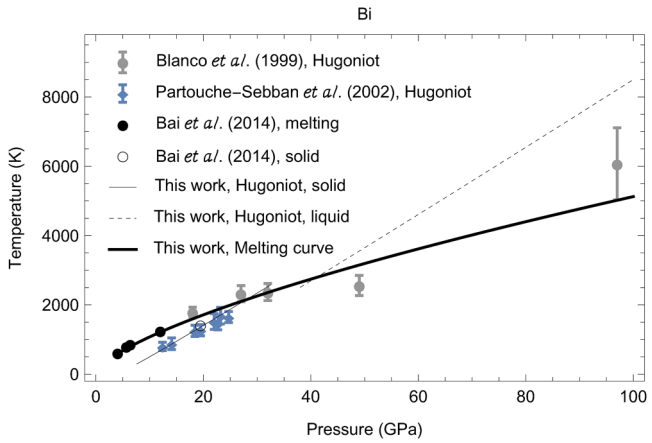

FIG. 9. The $0 \leq P \leq 100$ GPa portion of Fig. 8 containing the bcc-Bi principal Hugoniots from Refs. 10 and 11, and those calculated in our study (this work, solid/liquid). Also shown are the (P, T) final states on the release isentropes of Ref. 16. See the main text for more detail.

virtually coincides with the actual Bi-III–Bi-V-liquid triple point at (P, T) = (3.8 GPa, 569 K).[4] For each of the ten P_ms from Table I, except perhaps the first one, the corresponding T_ms are within 15 K of those given by Eq. (3). Thus, Eq. (3) is very accurate.

Figure 8 compares our theoretical melting curve of bcc-Bi, Eq. (3), to the theoretical melting curves available in the literature. For this comparison, we have chosen the melting curves of Refs. 12, 13 and 17. All the other theoretical melting curves are bounded by those of[13] from below and[17] from above, such that these "effective" lower and upper melting boundaries differ from each other by a factor of ≈2. We note good agreement of our theoretical melting curve of bcc-Bi with that of Ref. 17. The reason for this agreement is discussed below.

The low-P portion of the melting curve of bcc-Bi

Figure 9 details the $0 \leq P \leq 100$ GPa portion of Fig. 8. Here, we added the results of shock-compression experiments on Bi from the literature as well as our own theoretical Hugoniot of bcc-Bi,

$$T_{\mathrm{H}}(P) = 298 + 83.1\,(P - 7.6)^{1.03}, \tag{4}$$

shown in Fig. 9 as a thin line. Equation (4) is the best fit to a collection of ($P(V)$, $T(V)$) points obtained as those of the final states of QMD simulations at a number of fixed Vs. For these final states, the following condition is satisfied: $E - E_{\mathrm{ref}} = \frac{1}{2}\,(P + P_{\mathrm{ref}})\,(V_{\mathrm{ref}} - V)$ (which is one of the Rankine–Hugoniot relations), where the subscript "ref" indicates the reference point; in our case this point is the room-T Bi-III–Bi-V solid–solid transition point (7.6 GPa, 298 K).[5] Indeed, the calculations show[15] that the actual principal Hugoniot of Bi passes virtually across the Bi-III–Bi-V solid–solid transition point (the gray dashed line in Fig. 1 of Ref. 15). Thus, this point can indeed be taken as the starting point of the bcc-Bi principal Hugoniot.

To obtain the P–T conditions of the Bi Hugoniot melting, we also need to estimate its liquid Hugoniot. This is done by properly correcting Eq. (4) taking into account the difference in the volumes of liquid and solid bcc-Bi. Specifically, at melting the system volume increases from V_{sol} to V_{liq}. However, in *NVE* QMD simulations, volume is fixed and this volume change manifests itself as an increase in P, from P_{sol} to P_{liq}, which can be clearly seen in Figs. 4 and 6. The value of $\Delta V \equiv V_{\mathrm{liq}} - V_{\mathrm{sol}}$ can be obtained from ($V = V_{\mathrm{sol}}$) (i) $P_{\mathrm{sol}}(V) = P_{\mathrm{liq}}(V + \Delta V) = P_{\mathrm{liq}}(V) + dP_{\mathrm{liq}}/dV\,\Delta V$ and (ii) $P_{\mathrm{liq}}(V) = P_{\mathrm{sol}}(V) + \Delta P$. Hence, $\Delta V = V\Delta P/B$, where $B = -V dP_{\mathrm{liq}}/dV$ is the bulk modulus of liquid, etc. The resulting liquid Hugoniot is shown in Fig. 9 as a dashed line. The (P, T) points at which the solid and liquid Hugoniots cross the melting curve, Eq. (3), are, respectively, those of the beginning and end of the Hugoniot melting: [in (GPa, K)] (28, 2150) and (41, 2790).

Figure 9 also shows the (P, T) final states on the release isentropes of Ref. 16. Those identified in Ref. 16 as liquid or a solid–liquid mixture are indicated as "melting" in Fig. 9. As clearly seen, these (P, T) points virtually lie on our theoretical melting curve. We also note excellent agreement of our theoretical Hugoniot of bcc-Bi with that of Ref. 11 (blue points with error bars in Fig. 9) as well as the solid final state on the release isentrope of Ref. 16 (empty circle in Fig. 9).

DISCUSSION OF THE RESULTS

Our theoretical melting curve of bcc-Bi, Eq. (3), appears to be in excellent agreement with the final states on the release isentropes of Ref. 16 but with only one of several other theoretical melting curves available in the literature, namely, that of Ref. 17. At a P of 50 GPa (its highest P) it is higher than ours by a mere 100 K. Here, we clarify the reason for this agreement of the two melting curves which will lend further support for both of them and predict the behavior of the melting curve of[17] to pressure beyond 50 GPa.

The calculation of Ref. 17 is done in the so-called mean-field potential (MFP) approach developed in a series of papers by Wang in the early-2000s; see, e.g., Refs .[45–47] It was specifically applied to the study of melting curves.[48] The MFP approach to melting curves basically consists of a very careful determination of the Grüneisen gamma using DFT-based computational tools, and the subsequent calculation of $T_m(\rho)$ via $d\ln T_m(\rho)/d\ln\rho = 2(\gamma(\rho) - 1/3)$, i.e., in the Lindemann approach. Further analysis has revealed that, under certain approximations, the same Grüneisen gamma determines the ρ-dependence of the cold shear modulus, $G(\rho, 0)$;[49] specifically, $d\ln G(\rho, 0)/d\ln\rho = 2\gamma(\rho) + 1/3$. Thus, the above two relations give $G(\rho, 0)/(\rho \cdot T_m(\rho)) = \text{const.}$, which can be considered as the MFP melting curve equation. Using the thermoelasticity model of Preston and Wallace,[50] $G(\rho, T) = G(\rho, 0)(1 - \alpha T/T_m(\rho))$, and also assuming that the thermoelastic softening parameter α is density-independent, the above MFP melting curve equation can be rewritten as $G(\rho, T_m(\rho))/(\rho \cdot T_m(\rho)) = \text{const.}$, in agreement with the dislocation-mediated melting theory.[51,52]

The cold shear modulus of bcc-Bi was theoretically calculated in Ref. 41 up to ~200 GPa. Using our theoretical melting curve of bcc-Bi along with the results of Ref. 41, we found out that the value of the $G(\rho, 0)/(\rho \cdot T_m(\rho))$ decreases very slow with increasing ρ, i.e., it is not a constant, for which the most likely reason is the constancy of $G(\rho, T_m(\rho))/(\rho \cdot T_m(\rho))$ but a very weak ρ-dependence of the thermoelastic softening parameter. Such a very weak ρ-dependence of α occurs, e.g., for Mo, Ta, and W.[53] Nonetheless, we can calculate the MFP melting curve of bcc-Bi, given by $G(\rho, 0)/(\rho \cdot T_m(\rho)) = \text{const.}$, and compare it to that of.[17] This MFP curve is shown in Fig. 10 in the ρ–T coordinates along with ours given by Eq. (3).

The MFP melting curve virtually coincides with that of[17] converted to the ρ–T coordinates. In particular, it is ~100 K higher than ours at ~15 g/cm^3 (~50 GPa). At ~15.5 g/cm^3, it becomes higher by ~200 K but then falls down and eventually is below ours by ~1000 K at ~300 GPa and beyond.

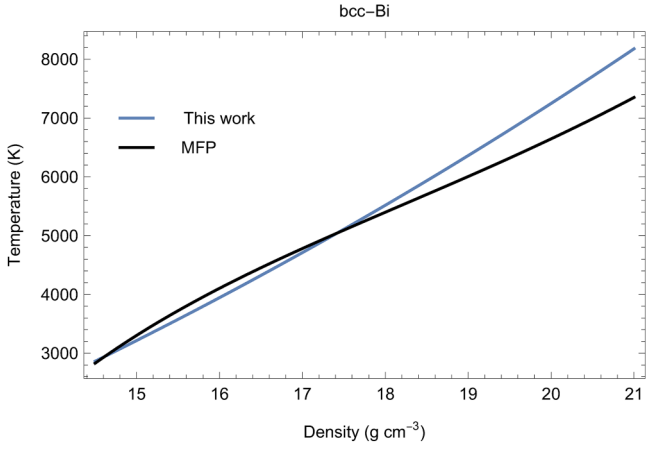

FIG. 10. Comparison of our *ab initio* melting curve of bcc-Bi (this work) to the theoretical melting curve of bcc-Bi calculated in the MFP approach (MFP).[17]

It is also worth comparing our theoretical results on the Hugoniot melting of bismuth to their experimental counterparts that can be found in the literature, especially because the earlier experiments suggested the P ranges for the Hugoniot melting that are quite different from each other, namely, ~30–45 GPa[10] and ~18–28 GPa.[11] The recent paper by Gorman *et al.*[54] offers a very careful femtosecond x-ray diffraction (XRD) study of shock-compressed Bi and its melting on the Hugoniot. Their results reveal that the XRD signal at 17 GPa corresponds to solid bcc-Bi, in agreement with the assessment of Ref. 55 that under shock compression Bi remains solid up to at least 17 GPa. The signatures of liquid appear at $P \sim 20$ GPa. At 24(2)–27(3) GPa a combined bcc-Bi–liquid signal is detected, in agreement with 28 GPa as the starting point of the Hugoniot melting in our theoretical calculations. A pure liquid signal is detected at 41(4) GPa, again in agreement with our end point of the Hugoniot melting of 41 GPa.

The final point that we wish to address here is whether bcc-Bi is the physical phase of bismuth in the megabar pressure range (1 Mbar = 100 GPa). The detailed study of the phase diagram of Bi, specifically, determining whether there exists another solid phase of Bi which melts higher than bcc-Bi and is, therefore, more stable than the latter, is well beyond the scope of this work. However, the stability of bcc-Bi can be given some considerations. Specifically, one can solidify liquid Bi into a final solid state and examine whether it possesses bcc or another structure. This procedure constitutes the so-called inverse Z method described in detail in Ref. 36 which is very useful for the study of the relative thermodynamic stability of different solid phases of a material. Since the solidification kinetics is approximately governed by the factor $\exp\{\Delta G/T_s\}$, where $\Delta G \equiv G_l - G_s$ is the liquid-solid Gibbs total free energy difference at the solidification temperature T_s, in the case of several energetically competitive solid phases the most stable solid phase has the largest ΔG and is, therefore, the fastest to solidify. Hence, the inverse Z method is expected to yield the most stable solid phase at a given (P, T). We prepared two liquid supercell, by melting 512-atom $(8 \times 8 \times 8)$ supercells of simple-cubic structure with lattice constants of 2.54 Å and 2.38 Å. These supercells have the same volumes as the bcc ones with lattice constants of, respectively, 3.2 Å and 3.0 Å. With the corresponding T_ms from Table I, the $0 - T_m$ intervals of T correspond to P intervals of, respectively, ~150–200 and 350–400 GPa (Fig. 2 and Table I). We carried out solidification simulations at a set of (fixed) Ts of 1250, 2500, 3750, 5000, and 6250 K for $a = 2.54$ Å, and 2000, 4000, 6000, 8000, and 10 000 K for $a = 2.38$ Å. Since for bcc-Bi with $a = 3.2$ Å, $T_m = 8340$ K (Table I), the highest T at which liquid of the same volume can solidify is $\sim 0.85\, T_m \simeq 7100$ K.[36] This is why 6250 K was chosen as the highest T for our solidification simulations of the $a = 2.54$ Å supercell. Similarly, for bcc-Bi with $a = 3.0$ Å, $T_m = 1313013\,130$ K, hence the highest solidification T is $\simeq 1110011\,100$ K, which explains the choice of 10 000 K as the highest T for our solidification simulations of the $a = 2.38$ Å supercell. For a total of 10 inverse Z runs, typical simulation time was 20 000 time steps of 1 fs each, i.e., 20 ps per run. Figure 11 shows the RDFs of the five final states of these simulations of the $a = 2.54$ Å supercell. As clearly seen, all the RDFs are similar to each other and correspond to the bcc structure (cf. RDF of bcc-Bi in Fig. 7).

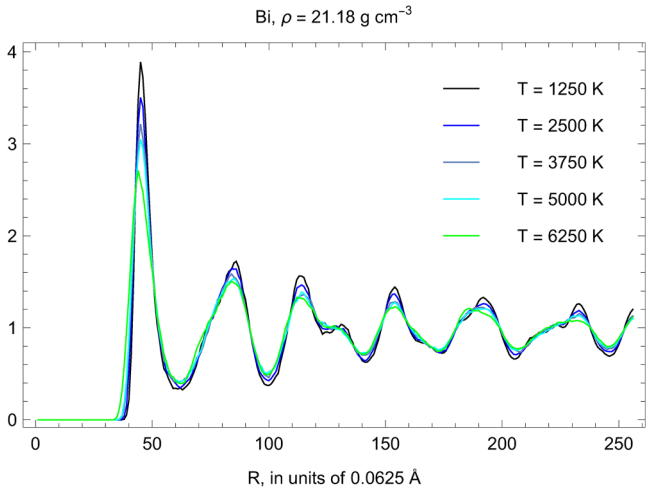

FIG. 11. Radial distribution functions (RDFs) of the final states of the solidification of liquid Bi at a set of fixed temperatures indicated as the corresponding *T*s.

The outcome of the solidification simulations of the $a = 2.38$ Å supercell is exactly the same: at all five *T*s the final solid state is bcc. Thus, the results of our inverse Z simulations imply the thermodynamic stability of bcc-Bi in the *T* range ~0–0.85 T_m, at least up to a pressure of ~400 GPa. In other words, if there exists another solid phase of Bi on its phase diagram in the megabar range, it can only be a sub-solidus phase, i.e., the phase that Bi melts from. Such a phase cannot be found in inverse Z simulations (as they do not apply to $T > \sim T_m$), hence both its detection and the determination of its physical properties require additional more detailed study. The study of the phase diagram of Bi in the megabar range will be undertaken in our subsequent research.

CONCLUDING REMARKS

Let us now summarize the results of our theoretical study on the melting curve of bcc-Bi.

We have presented the *ab initio* melting curve of body-centered cubic bismuth obtained from QMD simulations using the Z method implemented with VASP, Eq. (3). It starts at the Bi-III–Bi-V-liquid triple point of $(P, T) = (3.8\ \text{GPa}, 569\ \text{K})$ and extends to a *P* of 400 GPa (and a *T* of ~1350013 500 K), although Eq. (3) is very likely valid to much higher pressures. Of all the melting curves that currently exist in the literature, ours is in good agreement with the only one, namely, that of Ref. 17 which was calculated in the MFP approach. We have clarified the reasons for this agreement which lends further support to each of the two theoretical melting curves.

We have calculated the cold equation of state of bcc-Bi, Eq. (1), which appears to be in excellent agreement with both the experimental measurements and independent theoretical calculations.

The thermal equation of state for bcc-Bi also presented in this work, Eq. (2), appears to be in good agreement with both the available (room-*T*) experimental data and QMD melting simulations.

Our theoretical Hugoniot of Bi, Eq. (4) (and its counterpart for liquid Bi shown in Fig. 9) are associated with the *P* interval of the Hugoniot melting which is in good agreement with the most recent experimental studies on shock-compressed Bi of Refs. 54 and 55.

The EOS of bcc-Bi, Eqs. (1) and (2), constitutes the bismuth pressure standard. As discussed above, it is virtually an ideal pressure standard because it is (i) structurally stable in an exceptionally wide pressure interval of up to at least 300 GPa, (ii) nonradioactive, (iii) produces a strong XRD signal, (iv) possesses a bare minimal nonhydrostaticity compared to the vast majority of the other pressure standards such as Pt, Au, etc., and (v) its bulk modulus is much smaller than that of most of the other standards; hence, under the same *P* its volume change will be larger and thus the precision of the determination of *P* higher. The *T* range for the application of bcc-Bi as a standard (i.e., the *T* extent of bcc-Bi) is bounded by $0 \le T \le T_m(P)$ at any fixed *P*; with $T_m(P)$ given by Eq. (3), is as wide as those of the other typical standards. For instance, Fig. 16 of Ref. 56 shows that the seven 3rd row transition metals Re, Os, Ta, W, Ir, Pt, and Au that are typically used as pressure standards have T_m in the range of ~5500 K (Au) to 7500 K (Re) at a *P* of 100 GPa. In view of Eq. (4), for bcc-Bi $T_m(100\ \text{GPa})$ ~5200 K, albeit slightly lower than 5500 K of Au, is essentially in the same *T* range. Moreover, at 500 GPa, bcc-Bi melts only 1000 K below Re (15413 K vs 16 413 K), and at higher *P* its melting curve is (quasi-)parallel to that of Re because the two exponents of the corresponding SG forms are virtually identical (for Re, $T_m(P) = 3460\,(1 + P/58.5)^{0.69}$ [56]), and the corresponding prefactors are very close to each other: $568.9/4.05^{0.685} \approx 218$ for bcc-Bi vs $3460/58.5^{0.69} \approx 209$ for Re. Although at ambient *P* Re has the second highest T_m (behind W), at $P > \sim 30$ GPa it is the highest melter among the elements of the 3rd row of the periodic table. But the second highest melter, behind Re, at $P > \sim 500$ GPa appears to be bcc-Bi.

Thus, body-centered cubic bismuth will be an exceptional pressure standard for the future high pressure and high temperature experiments. In addition to being an essential component for the *P*-*T* characterization of this standard, the melting curve of bcc-Bi calculated by ourselves in *ab initio* approach and presented in this work will contribute to the study on melting systematics for the elements of the 3rd row of the periodic table.

ACKNOWLEDGMENTS

The work was done under the auspices of the U.S. DOE/NNSA. The QMD simulations were performed on the LANL cluster Chicoma as part of the Institutional Computing projects w22_phadiagractox and w24_phadiagractox. D.E. acknowledges financial support from Spanish Ministerio de Ciencia, Innovación y Universidades (Grants Nos. PID2022-138076NB-C41 and RED2018-102612-T) and Generalitat Valenciana (Nos. PROMETEO CIPROM/2021/075-GREENMAT and MFA/2022/007). S.A. thanks the Generalitat Valenciana for the CIDEGENT Grant No. CIDEXG/2022/6.

AUTHOR DECLARATIONS

Conflict of Interest

The authors have no conflicts to disclose.

Author Contributions

Leonid Burakovsky: Investigation (equal); Methodology (equal); Project administration (equal); Writing – original draft (equal). **Daniel A. Rehn:** Investigation (equal); Methodology (equal); Writing – review & editing (equal). **Simone Anzellini:** Investigation (equal); Methodology (equal); Writing – review & editing (equal). **Daniel Errandonea:** Investigation (equal); Methodology (equal); Writing – review & editing (equal).

DATA AVAILABILITY

The data that support the findings of this study are available from the corresponding author upon reasonable request.

REFERENCES

[1]X. Du, S.-W. Tsai, D. L. Maslov, and A. F. Hebard, "Metal-insulator-like behavior in semimetallic bismuth and graphite," Phys. Rev. Lett. **94**, 166601 (2005). and references therein.

[2]E. N. Gribanov, O. I. Markov, and Y. V. Khripunov, "When does bismuth become a semimetal?," Nanotechnol. Russ. **6**, 593 (2011). and references therein.

[3]B. N. Galimzyanov, A. A. Tsygankov, A. A. Suslov, V. I. Lad'yanov, and A. V. Mokshin, "Quasi-stable structures in equilibrium dense bismuth melt: Experimental and first principles theoretical studies," Scr. Mater. **235**, 115618 (2023).

[4]W. Klement, A. Jayaraman, and G. C. Kennedy, "Phase diagrams of arsenic, antimony, and bismuth at pressures up to 70 kbars," Phys. Rev. **131**, 632 (1963).

[5]S. Ono, "High-pressure phase transition of bismuth," High Pres. Res. **38**, 414 (2018).

[6]C. V. Storm, J. D. McHardy, M. J. Duff, S. G. MacLeod, E. F. O'Bannon, and M. I. McMahon, "The stress state in bismuth to 298 GPa and its use as a pressure transmitting medium and pressure marker at multi-megabar pressures," J. Appl. Phys. **133**, 245904 (2023).

[7]A. Dewaele, P. Loubeyre, and M. Mezouar, "Equations of state of six metals above 94 GPa," Phys. Rev. B **70**, 094112 (2004).

[8]L. Xu, Y. Bi, X. Li, Y. Wang, X. Cao, L. Cai, Z. Wang, and C. Meng, "Phase diagram of tin determined by sound velocity measurements on multi-anvil apparatus up to 5 GPa and 800 K," J. Appl. Phys. **115**, 164903 (2014).

[9]C. Su, Y. Liu, Z. Wang, W. Song, P. D. Asimow, H. Tang, and H. Xie, "Equation of state of liquid bismuth and its melting curve from ultrasonic investigation at high pressure," Phys. B **524**, 154 (2017). and references therein.

[10]E. Blanco, J. M. Mexmain, and P. Chapron, "Temperature measurements of shock heated materials using multispectral pyrometry: Application to bismuth," Shock Waves **9**, 209 (1999).

[11]D. Partouche-Sebban, D. B. Holtkamp, J. L. Pélissier, J. Taboury, and A. Rouyer, "An investigation of shock induced temperature rise and melting of bismuth using high-speed optical pyrometry," Shock Waves **11**, 385 (2002).

[12]J. L. Pélissier and N. Wetta, "A model-potential approach for bismuth (I). Densification and melting curve calculation," Phys. A **289**, 459 (2001).

[13]D. K. Belashchenko, "Molecular dynamics calculation of properties of liquid lead and bismuth under shock compression," High Temp. **55**, 370 (2017).

[14]D. Mukherjee, B. D. Sahoo, K. D. Joshi, and S. C. Gupta, "On equation of state, elastic, and lattice dynamic stability of bcc bismuth under high pressure: *Ab initio* calculations," J. Appl. Phys. **115**, 053702 (2014).

[15]G. A. Cox, "A multi-phase equation of state for bismuth," AIP Conf. Proc. **955**, 151 (2007).

[16]J. Bai, J. Yu, and T. Wang, "Numerical investigation of bismuth unloading solidification with abnormal melting characteristic," World J. Mech. **4**, 203 (2014).

[17]Y.-H. Li, J. Z. Chang, X. M. Li, Y. Y. Yu, C. D. Dai, and L. Zhang, "Multiphase equation of states of solid and liquid phases for bismuth," Acta Phys. Sin. **61**, 206203 (2012).

[18]G. Kresse and J. Furthmüller, "Efficiency of *ab initio* total energy calculations for metals and semiconductors using a plane-wave basis set," Comput. Mater. Sci. **6**, 15 (1996).

[19]G. Kresse and J. Furthmüller, "Efficient iterative schemes for *ab initio* total-energy calculations using a plane-wave basis set," Phys. Rev. B **54**, 11169 (1996).

[20]M. Woodcox, J. Young, and M. Smeu, "*Ab initio* investigation of the temperature-dependent elastic properties of Bi, Te and Cu," J. Phys. Cond. Mat. **32**, 485902 (2020).

[21]J. P. Perdew, K. Burke, and M. Ernzerhof, "Generalized gradient approximation made simple," Phys. Rev. Lett. **77**, 3865 (1996); erratum, *ibid.* **78**, 1396 (1997).

[22]I. Timrov, *Ab initio* study of plasmons and electron-phonon coupling in bismuth: From free-carrier absorption towards a new method for electron energy-loss spectroscopy, Ph.D. thesis (ParisTech, 2013). See https://pastel.hal.science/pastel-00823758.

[23]J. P. Perdew, A. Ruzsinszky, G. I. Csonka, O. A. Vydrov, G. E. Scuseria, L. A. Constantin, X. Zhou, and K. Burke, "Restoring the density-gradient expansion for exchange in solids and surfaces," Phys. Rev. Lett. **100**, 136406 (2008).

[24]G. X. Zhang, A. M. Reilly, A. Tkatchenko, and M. Scheffler, "Performance of various density-functional approximations for cohesive properties of 64 bulk solids," New J. Phys. **20**, 063020 (2018).

[25]L. Cheng, H. Liu, X. Tan, J. Zhang, J. Wei, H. Lv, J. Shi, and X. Tang, "Thermoelectric properties of a monolayer bismuth," J. Phys. Chem. C **118**, 904 (2014).

[26]J. Akola, N. Atodiresei, J. Kalikka, J. Larrucea, and R. O. Jones, "Structure and dynamics in liquid bismuth and Bi_n clusters: A density functional study," J. Chem. Phys. **141**, 194503 (2014).

[27]F. Schindler, Z. Wang, M. G. Vergniory, A. M. Cook, A. Murani, S. Sengupta, A. Y. Kasumov, R. Deblock, S. Jeon, I. Drozdov, and H. Bouchiat, "Higher-order topology in bismuth," Nat. Phys. **14**, 918 (2018).

[28]P. H. T. Philipsen and E. J. Baerends, "Relativistic calculations to assess the ability of the generalized gradient approximation to reproduce trends in cohesive properties of solids," Phys. Rev. B **61**, 1773 (2000).

[29]T. Hirahara, T. Nagao, I. Matsuda, G. Bihlmayer, E. V. Chulkov, Y. M. Koroteev, P. M. Echenique, M. Saito, and S. Hasegawa, "Role of spin-orbit coupling and hybridization effects in the electronic structure of ultrathin Bi films," Phys. Rev. Lett. **97**, 146803 (2006).

[30]N. Fukumoto, R. Ohshima, M. Aoki, Y. Fuseya, M. Matsushima, E. Shigematsu, T. Shinjo, Y. Ando, S. Sakamoto, M. Shiga, and S. Miwa, "Observation of large spin conversion anisotropy in bismuth," Proc. Natl. Acad. Sci. U.S.A. **120**, e2215030120 (2023).

[31]B. Arnaud, S. Lebègue, and G. Raffy, "Anisotropic thermal expansion of bismuth from first principles," Phys. Rev. B **93**, 094106 (2016).

[32]Y. Zhao, S. Clément, J. Haines, and R. Viennois, "Lattice dynamics study of elemental bismuth under high pressure," J. Phys. Chem. C **124**, 26659 (2020).

[33]Y. F. Zhao *et al.*, see https://arxiv.org/pdf/1903.02773.pdf for "A first principles study of high pressure phase diagram of bismuth at 0 ∼ 14 GPa based on structure search and quasi-harmonic approximation."

[34]G. Kresse (Vienna), private communication (2017).

[35]A. B. Belonoshko, N. V. Skorodumova, A. Rosengren, and B. Johansson, "Melting and critical superheating," Phys. Rev. B **73**, 012201 (2006).

[36]L. Burakovsky, S. P. Chen, D. L. Preston, and D. G. Sheppard, "Z methodology for phase diagram studies: Platinum and tantalum as examples," J. Phys. Conf. Ser. **500**, 162001 (2014).

[37]L. Burakovsky, N. Burakovsky, and D. L. Preston, "*Ab initio* melting curve of osmium," Phys. Rev. B **92**, 174105 (2015).

[38]F. Birch, "Finite elastic strain of cubic crystals," Phys. Rev. **71**, 809 (1947).

[39]F. D. Murnaghan, "The compressibility of media under extreme pressures," Proc. Natl. Acad. Sci. USA **30**, 244 (1944).

[40]Y. Akahama, H. Kawamura, and A. Singh, "Equation of state of bismuth to 222 GPa and comparison of gold and platinum pressure scales to 145 GPa," J. Appl. Phys. **92**, 5892 (2002).

[41]G. Gutiérrez, E. Menéndez-Proupin, and A. Singh, "Elastic properties of the bcc structure of bismuth at high pressure," J. Appl. Phys. **99**, 103504 (2006).
[42]D. J. Campbell, D. T. Sneed, E. F. O'Bannon III, P. Söderlind, and Z. Jenei, "Refined room-temperature equation of state of Bi up to 260 GPa," Phys. Rev. B **107**, 224104 (2023).
[43]X. Fan, S. Xiang, and L. Cai, "Temperature dependence of bismuth structures under high pressure," Chin. Phys. B **31**, 056101 (2022).
[44]A. B. Belonoshko, J. Fu, and G. Smirnov, "Free energies of iron phases at high pressure and temperature: Molecular dynamics study," Phys. Rev. B **104**, 104103 (2021); erratum, *ibid.* **105**, 159903 (2022).
[45]Y. Wang and L. Li, "Mean-field potential approach to thermodynamic properties of metal: Al as a prototype," Phys. Rev. B **62**, 196 (2000).
[46]Y. Wang, R. Ahuja, and B. Johansson, "Reduction of shock-wave data with mean-field potential approach," J. Appl. Phys. **92**, 6616 (2002).
[47]Y. Wang, R. Ahuja, and B. Johansson, "Mean-field potential approach to the quasiharmonic theory of solids," Int. J. Quantum Chem. **96**, 501 (2004).
[48]Y. Wang, R. Ahuja, and B. Johansson, "Melting of iron and other metals at Earth's core conditions: A simplified computational approach," Phys. Rev. B **65**, 014104 (2001).
[49]L. Burakovsky, D. L. Preston, and Y. Wang, "Cold shear modulus and Grüneisen parameter at all densities," Solid State Commun. **132**, 151 (2004).
[50]D. L. Preston and D. C. Wallace, "A model of the shear modulus," Solid State Commun. **3**, 277 (1992).
[51]L. Burakovsky and D. L. Preston, "Analysis of dislocation mechanism for melting of elements," Solid State Commun. **7**, 341 (2000).
[52]L. Burakovsky, D. L. Preston, and R. R. Silbar, "Analysis of dislocation mechanism for melting of elements: Pressure dependence," J. Appl. Phys. **88**, 6294 (2000).
[53]L. Burakovsky, D. J. Luscher, D. Preston, S. Sjue, and D. Vaughan, "Generalization of the unified analytic melt-shear model to multi-phase materials: Molybdenum as an example," Crystals **9**, 86 (2019).
[54]M. G. Gorman, A. L. Coleman, R. Briggs, R. S. McWilliams, D. McGonegle, C. A. Bolme, A. E. Gleason, E. Galtier, H. J. Lee, E. Granados, and M. Śliwa, "Femtosecond diffraction studies of solid and liquid phase changes in shock-compressed bismuth," Sci. Rep. **8**, 16927 (2018).
[55]R. Briggs, M. J. Suggit, M. G. Gorman, A. Coleman, R. Heathcote, A. Higginbotham, S. Patel, J. S. Wark, and M. I. McMahon, "Phase transitions in shock compressed bismuth identified using single photon energy dispersive x-ray diffraction (SPEDX)," J. Phys. Conf. Ser. **950**, 042038 (2017).
[56]L. Burakovsky, N. Burakovsky, D. L. Preston, and S. Simak, "Systematics of the third row transition metal melting: The hcp metals rhenium and osmium," Crystals **8**, 243 (2018).